

High sensitivity and resolution hole-phase-shifted fibre Bragg grating sensor

J. F. Algorri,^{1,2,3,*} L. Rodriguez-Cobo,² and J.M López-Higuera,^{1,2,3}

¹Photonics Engineering Group, Universidad de Cantabria, 39005, Santander, Spain

²CIBER-bbn, Instituto de Salud Carlos III, 28029, Madrid, Spain

³Instituto de Investigación Sanitaria Valdecilla (IDIVAL), 39011, Santander, Spain

*algorrijf@unican.es

Abstract: This work introduces a new sensor type characterised by high sensitivity and resolution. The sensor utilises a fibre Bragg grating (FBG) with a perforated through-hole in the middle, resulting in a hole-phase-shifted FBG sensor.

© 2023 The Author(s)

1. Introduction

Optical fibre optofluidic sensors are a type of optofluidic technology that combines photons and microfluidics to produce a more powerful and integrated platform for sensing. This kind of sensors has several advantages over traditional sensors, including a compact structure, immunity to electromagnetic interference, low sample consumption, high sensitivity, and real-time dynamic response. In recent years, there has been significant research progress in developing sensors based on various sensing mechanisms, including microcavities, microfibers, and surface plasmon resonance. These sensing mechanisms have been widely used in various applications, including medical diagnosis, environmental monitoring, and food safety.

The optical fibres suitable for optofluidic sensors are numerous and diverse. Still, they can be broadly categorized into two types: optical fibres with microfluidic channels [1], and optical fibres that can be integrated into microfluidic channels [2]. The latter group includes microfiber, thin fibre, and D-shaped fibre. Optical fibres with microfluidic channels enable the integration of light and fluid within the fibre, resulting in significant benefits such as a long interaction distance between light and microfluidics, a compact structure, and easy coupling of optical signals, leading to their rapid development. On the other hand, microcavities are a type of optofluidic sensor that uses a small cavity to trap light and enhance the interaction between the light and the sample. This results in high sensitivity and selectivity for detecting gases and liquids. Microcavities have been used in various applications, including the detection of proteins, DNA, and viruses. The capillary optical fibre's large microfluid channel makes it convenient to input and output gases or liquids. Moreover, it has a flexible structure and simple preparation, which are advantageous. Various structures, such as microcavities [3], hollow-core microfiber (HCMF) [4], microbottle resonators [5], and microbubble resonators [6], have been developed to meet the demands of different sensing applications. In the past, microbubbles have been used as interferometers, micro-optical resonators, or microfluidic reservoirs, with circular microbubbles being the most commonly used [7]. However, near-square cavities or those with a pronounced elliptical shape have been achieved using fusion splicers or tapered fibres [8–10].

This work presents a novel approach to achieving high sensitivity to the surrounding medium using a microcavity that can be easily fabricated. By inscribing a fibre Bragg grating (FBG) and making a perforation from side to side in the middle of the FBG, a high sensitivity and resolution hole-phase-shifted fibre Bragg grating sensor is obtained. The phase change in this design is unique because it is performed within the microhole, which is communicated with the surrounding medium. A theoretical model has been developed to analyse and optimise the sensor response. The sensor can produce reflection peaks with extremely narrow line widths by adjusting the FWHM as a function of the FBG length. These spectral features contribute to the high resolution of the sensor. Furthermore, the hole cavity exhibits significant sensitivity to refractive index and strain variations.

2. Structure and theoretical background

Previous reports have described the fabrication process of in-fibre air bubbles, which requires multiple steps and the use of two cleaved fibre sections. First, a small hole is created in the end-face of one section using an fs laser, typically in the core to ensure the bubble is centred in the fibre. The size of the microhole determines the size of the subsequent circular bubble generated by an electric arc discharge during splicing. In this work, we simplify this process by using a single-mode fibre with an FBG inscribed and a perforation created in the middle using fs

laser or micro-machining, thereby avoiding the need to place a bubble in the middle. A schematic depiction of the resulting structure is shown in Figure 1.

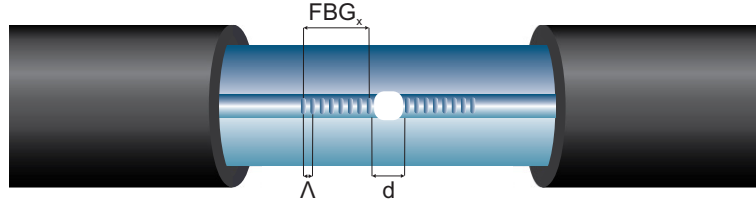


Fig. 1. Top view of the proposed structure, a through hole is made in the middle of the FBG.

We employ the Coupled-Mode Theory (CMT) [11] and Transfer Matrix Method (TMM) [12] to simulate the proposed structure. CMT and TMM are widely used due to their accuracy and ease of implementation for studying light propagation in weakly coupled waveguide media. CMT assumes that the transverse components of the electric field in coupled structures, such as waveguides with gratings, can be expressed as a linear superposition of ideal modes of an unmodified waveguide. The transverse component of the electric field along the grating can be represented as the sum of the forward and backward propagation modes [13]:

$$\vec{E}_t(x, y, z, t) = \sum_i [A_j(z) \exp(i\beta_j z) + B_j(z) \exp(-i\beta_j z)] \cdot \vec{e}_{jt}(x, y) \exp(i\omega t) \quad (1)$$

The j -th mode's forward and backward travelling amplitudes, $A_j(z)$ and $B_j(z)$ respectively, are gradually varying, while the field distribution $\vec{e}_{jt}(x, y)$ describes the transverse mode fields that represent the radiation LP modes and cladding modes. The propagation constant of the j -th mode is denoted as β , and the angular frequency as ω . In an ideal waveguide, these orthogonal modes do not transfer energy. However, introducing a dielectric perturbation causes mode coupling along the propagation axis, which can be described by the complex equations dA_j/dz and dB_j/dz . To simplify these equations, the synchronous approximation can be used, which neglects the rapidly oscillating terms on the right-hand side of the differential equations, as they do not contribute significantly to the amplitudes' growth and decay. Consequently, the mode evolution is described by varying amplitudes along the grating length (L) as defined by Eqs. (2) and (3).

$$\frac{dR}{dz} = i\vartheta R(z) + i\kappa S(z) \quad (2)$$

$$\frac{dS}{dz} = -i\vartheta S(z) - i\kappa^* R(z) \quad (3)$$

where $R(z) \equiv A(z) \exp(i\delta z - \phi/2)$ (the forward propagating wave) and $S(z) \equiv B(z) \exp(-i\delta z + \phi/2)$ (the backward propagating wave). See Ref. [7] for more details of equations.

To solve the problem at hand, the TMM will be utilized, which involves dividing the grating into smaller sections with uniform coupling properties. The structure will be split into three uniform sections, and the field amplitudes after traversing each section will be denoted as R_x and S_x . The propagation through each uniform FBG can be described using \mathcal{F}_{Gx} , while the hole can be modelled as a phase-shift matrix \mathcal{F}_B . Finally, the transfer matrix of the whole structure can be expressed as $\mathcal{F} = \mathcal{F}_{G1} \cdot \mathcal{F}_B \cdot \mathcal{F}_{G2}$ where the reflectivity and transmissivity are expressed by $r = \mathcal{F}_{21}/\mathcal{F}_{11}$ and $t = 1/\mathcal{F}_{11}$. In order to consider the strain effect, it has to be considered that several parameters are affected, e.g. the period and length of the grating, the width of the hole and the effective index of the core due to the photo-elastic effect. Assuming the fibre is only free to deform in the transverse plane, its radial strain ε_r driven by the axial strain: $\varepsilon_r = -\nu \varepsilon_z$, where ν is the Poisson's ratio of the fibre. In this case and approximating that the effective index change is equivalent to the change in the bulk material's index, the variation is expressed by Eq. 4 [14, 15]. It has to be considered that silica optical fibres have $\nu = 0.17$, $p_{11} = 0.121$ and $p_{12} = 0.270$ [14].

$$\frac{\Delta n_{eff}}{n_{eff}} + \varepsilon_z = \left\{ 1 - \frac{n_{eff}^2}{2} [p_{12} - \nu(p_{11} + p_{12})] \right\} \varepsilon_z \quad (4)$$

3. Results

The resonance wavelength of the sensor is mainly dependent on the period (Λ) of the fibre Bragg grating (FBG). In this particular case, the sensor is designed to achieve maximum transmittance at 1550 nm with air inside the

hole ($\Lambda = 531.55 \text{ nm}$). The diameter of the hole is critical to ensure an odd multiple of π phase shift between the two FBGs, which is necessary for the resonance to be centred. The effect of variations in the hole size on the resonance wavelength can be observed in Figure 1. As shown, a hole size of $50 \mu\text{m}$ is required to produce a resonance wavelength at 1550 nm when the refractive index inside the hole is $n_H = 1$. However, for small variations in hole size, the resonance position is periodic. This gives a certain error margin in the perforation as only phase shifts in the hole of $2 \cdot \pi$ lose the resonance wavelength. Concerning the FBG length, a size of 0.5 mm at each side of the hole is chosen (giving an FWHM of 14.5 pm). A study of the FBG length gives an exponential relation between FBG length and FWHM ($7 \cdot 10^{-9} \cdot e^{-1.2 \cdot 10^4 \cdot FBG_x}$), so the higher the FBG the narrower the response.

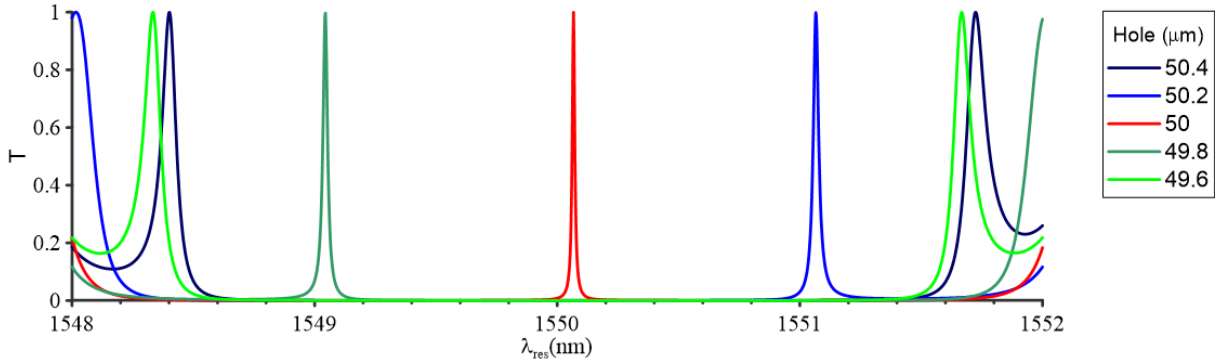


Fig. 2. Transmittance spectra for $n_H=1$ and several hole widths. Each FBG has a length of 0.5 mm

To investigate the impact of the refractive index within the hole, the spectral range used is limited to 1548.5 nm to 1551.8 nm to avoid double-side resonance. A noticeable discontinuity in the spectra is observed due to the shift of the side resonance from the upper to the lower part of the spectrum as the refractive index changes (caused by the phase oscillating produced by the hole between 0 to 2π). Although only the spectra corresponding to a refractive index ranging from 1 to 1.1 are displayed in Fig. 3(a), the curve is analogous for higher refractive indices, allowing the sensor to cover all refractive indices of gases and liquids up to 2 . However, a limited measurable range of 0.01 RIU is necessary. By selecting a hole size of $50 \mu\text{m}$, in Fig. 3(b) it is shown an example of the variation in the wavelength resonance, resulting from a change in the refractive index from 1.01 to 1.02 . The resulting sensitivity of 253 nm/RIU , which is suitable for gas sensing. The refractive index of several sensing gases falls within the interval from 1 to 1.001 , indicating that the resolution required for the proposed gas sensor should be in the order of 25 pm to detect index variations of 0.0001 . The chosen FBG length can detect these steps, with a FWHM of 14.5 pm . This resolution is attainable with many commercially available optical spectrum analyzers (OSA), with high-resolution models providing values down to 0.04 pm (e.g., the AP208x high-resolution OSA from APEX Technologies), which is three orders of magnitude lower than the 25 pm considered for the proposed sensor's operation. Additionally, the sensor's figure of merit ($\text{FoM} = S/\text{FWHM}$), is very high due to the narrow linewidth of resonances and high sensitivity ($\text{FoM} = 17.5 \cdot 10^4 \text{ RIU}^{-1}$).

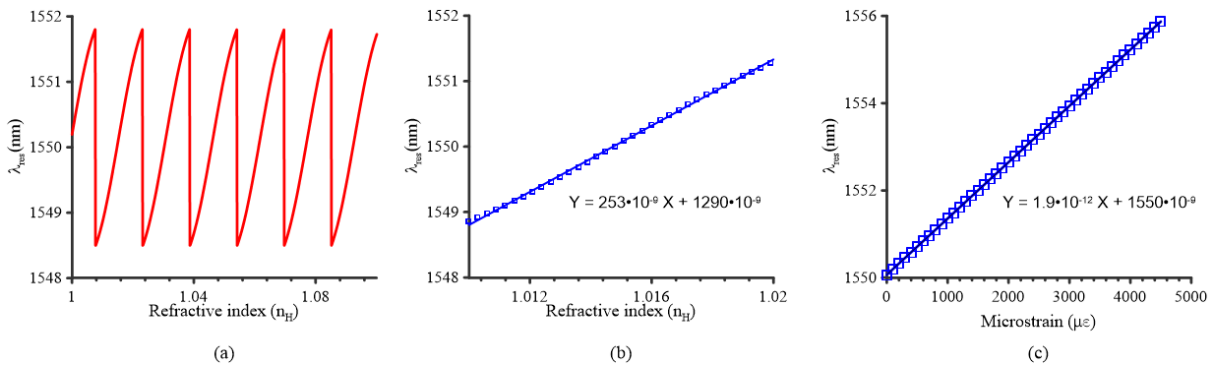


Fig. 3. (a) λ_{res} for several refractive indexes (a) $n_H = 1-1.1$ and (b) $n_H = 1.01-1.02$ (253 nm/RIU) (c) λ_{res} vs $\mu\epsilon$ ($S = 1.9 \text{ pm}/\mu\epsilon$). Each FBG has a length of 0.5 mm and the hole a width of $50 \mu\text{m}$

Finally, a study of the proposed sensor's strain effect is depicted in Fig. 3(c), which indicates a linear response from 0 to $5000 \mu\epsilon$ within the fibre's limits (the fracture strain of an optical fibre recoated with acrylate is 0.45%

and with polyimide 0.79% [16]. The sensitivity achieved is $1.9 \text{ pm}/\mu\epsilon$, which is twice the typical sensitivity of FBG sensors.

4. Conclusions

In conclusion, this paper presents a novel design for a gas-liquid sensor based on a microhole in an FBG. The proposed sensor is highly sensitive to changes in the surrounding refractive index and has a high resolution. The fabrication process is simple and requires only one cleaved fibre section, which makes it cost-effective and easy to implement. The results demonstrate the feasibility of the proposed design and its potential for various sensing applications. Specifically, a sensitivity of $253 \text{ nm}/\text{RIU}$ and an FoM = $17.5 \cdot 10^4 \text{ RIU}^{-1}$. This parameter can even be enhanced by modifying the FBG length. Also, a $1.9 \text{ pm}/\mu\epsilon$ sensitivity is obtained to changes in the strain, doubling the typical sensitivity of FBG sensors. Future work will focus on optimizing the sensor performance and exploring its applications in different fields.

Funding

MCIN/AEI/10.13039/501100011033, FEDER and EU NextGenerationEU/PRT funds of European Commission (PID2019-107270RB-C21, PDC2021-121172-C21 and TED2021-130378B-C21). J.F.A. received funding from MCIN of Spain under Juan de la Cierva-Incorporación.

References

1. M. Calcerrada, C. García-Ruiz, and M. González-Herráez, "Chemical and biochemical sensing applications of microstructured optical fiber-based systems," *Laser & Photonics Reviews* **9**(6), pp. 604–627, 2015.
2. Y. Zhao, X. Guang Hu, S. Hu, and Y. Peng, "Applications of fiber-optic biochemical sensor in microfluidic chips: A review," *Biosensors and Bioelectronics* **166**, p. 112447, 2020.
3. J. F. Algorri, B. García-Cámara, A. García-García, V. Urruchi, and J. M. Sánchez-Pena, "Fiber optic temperature sensor based on amplitude modulation of metallic and semiconductor nanoparticles in a liquid crystal mixture," *Journal of Lightwave Technology* **33**(12), pp. 2451–2455, 2015.
4. B. Li Li, D. Ran Li, J. Hui Chen, Z. Yong Liu, G. Hui Wang, X. Ping Zhang, F. Xu, and Y. Qing Lu, "Hollow core micro-fiber for optical wave guiding and microfluidic manipulation," *Sensors and Actuators B: Chemical* **262**, pp. 953–957, 2018.
5. R.-I. Stoian, B. K. Lavine, and A. Rosenberger, "ph sensing using whispering gallery modes of a silica hollow bottle resonator," *Talanta* **194**, pp. 585–590, 2019.
6. P. Roldán-Varona, L. Rodríguez-Cobo, and J. M. López-Higuera, "Reflection-based lab-in-fiber sensor integrated in a surgical needle for biomedical applications," *Optics Letters* **45**, pp. 5242–5245, sep 2020.
7. J. F. Algorri, P. Roldán-Varona, M. Ochoa, L. Rodríguez-Cobo, and J. M. López-Higuera, "Microfluidic sensor based on a microbubble-phase-shifted fibre bragg grating," *27th International Conference on Optical Fiber Sensors*, p. W4.60, Optica Publishing Group, 2022.
8. S. Liu, K. Yang, Y. Wang, J. Qu, C. Liao, J. He, Z. Li, G. Yin, B. Sun, J. Zhou, G. Wang, J. Tang, and J. Zhao, "High-sensitivity strain sensor based on in-fiber rectangular air bubble," *Scientific Reports* **5**, jan 2015.
9. C. R. Liao, D. N. Wang, and Y. Wang, "Microfiber in-line mach-zehnder interferometer for strain sensing," *Optics Letters* **38**, pp. 757–759, feb 2013.
10. C. Liao, F. Zhu, P. Zhou, and Y. Wang, "Fiber taper-based mach-zehnder interferometer for ethanol concentration measurement," *Micromachines* **10**, p. 741, oct 2019.
11. A. Yariv, "Coupled-mode theory for guided-wave optics," *IEEE Journal of Quantum Electronics* **9**(9), pp. 919–933, 1973.
12. M. Yamada and K. Sakuda, "Analysis of almost-periodic distributed feedback slab waveguides via a fundamental matrix approach," *Appl. Opt.* **26**, pp. 3474–3478, Aug 1987.
13. T. Erdogan, "Fiber grating spectra," *Journal of Lightwave Technology* **15**(8), pp. 1277–1294, 1997.
14. M. E.-S. R. Gafsi, "Analysis of induced-birefringence effects on fiber bragg gratings," *Opt. Fiber Technol.* **6**(3), p. 299–323, 2000.
15. C. S. M.S. Müller, "Analytical coherency matrix treatment of shear strained fiber bragg gratings," *Opt. Express* **22624**, 2009.
16. J.-M. Kim, C.-M. Kim, S.-Y. Choi, and B. Y. Lee, "Enhanced strain measurement range of an fbg sensor embedded in seven-wire steel strands," *Sensors* **17**(7), 2017.